IRAQI JOURNAL OF APPLIED PHYSICS
Vol. 22, No. 3, July-September 2026, pp. 441-446

Structural and Optical Characterization of Cerium Dioxide Thin Films Prepared and Doped with Carbon Nanotubes by Pulsed-Laser Deposition

Walaa H. Shaaban*
Kawkab D. Salim

Department of Physics,
College of Education for
Pure Sciences,
University of Tikrit,
Tikrit, IRAQ
*Corresponding author Email:
WHSueps91@st.tu.edu.iq

Thin films of pure cerium oxide (CeO_2) and CeO_2-doped with carbon nanotubes (CNTs) at (0.1, 0.3, and 0.5 wt.%) were fabricated on glass substrates using pulsed laser deposition (PLD). X-ray diffraction (XRD) confirmed polycrystalline films with preferred (111) orientation, and higher CNT doping resulted in broader peaks, indicating reduced crystallite size. Atomic force microscopy (AFM) and scanning electron microscopy (FE-SEM) revealed that increased doping decreased grain size and surface roughness, with mostly homogeneous grain distribution and minor agglomeration. UV–Visible spectroscopy showed decreased absorbance and a widening of the energy band gap from 2.71 eV (pure) to 3.14 eV (0.5 wt.% CNTs). These structural and optical modifications highlight the effectiveness of CNTs incorporation in tuning CeO_2 thin film properties. The observed changes suggest promising potential for tunable optical coatings, enhanced photocatalytic activity, and advanced gas sensing applications.

Keywords: Thin films; Pulsed-laser deposition; Cerium dioxide; Carbon nanotubes
Received: 7 November 2025; Revised: 8 January 2026; Accepted: 15 January 2026; Published: 1 July 2026

1. Introduction

Thin films are coatings of materials deposited on substrates such as glass, quartz, or silicon, with thicknesses typically smaller than 1 μm [1]. They play a crucial role in enhancing the properties of semiconductors, making them highly sensitive to external stimuli such as heat, light, and minor impurities [2]. This sensitivity renders semiconductors essential in a wide range of electronic applications. Among various deposition techniques, pulsed laser deposition (PLD) offers precise control over film thickness, stoichiometry, and morphology, making it suitable for fabricating high-quality thin films [3].

Cerium oxide (CeO_2) is a widely used metal oxide with applications ranging from catalysis to optical coatings. Its ability to form non-stoichiometric oxides allows for tuning structural and electronic properties, which is vital for advanced functional devices [4,5]. Carbon nanotubes (CNTs), particularly multiwalled CNTs, exhibit high surface area, excellent mechanical strength, and chemical stability, making them ideal candidates for enhancing semiconductor materials [6-8]. They consist of concentric layers of sp^2-hybridized carbon atoms arranged in cylindrical structures, enabling efficient charge transport and defect modulation [9]. Despite extensive studies on CeO_2 thin films, the impact of CNTs incorporation via PLD on their morphology and optical properties remains underexplored. Combining CNTs with CeO_2 is expected to reduce crystallite and grain sizes, enhance charge separation, and modify optical responses, offering potential applications in tunable optical coatings, photocatalysis, and gas sensing.

2. Experimental Work

Thin films of cerium oxide (CeO_2) and CeO_2 doped with multiwalled carbon nanotubes (MWCNTs; 10–20 nm diameter, 5-15 μm length, >95% purity, Sigma-Aldrich) were prepared. For all doped targets, the CeO_2 mass was kept constant at 2 g, and CNTs were added at (0.1, 0.3, and 0.5 wt.%). Materials were weighed using a Mettler A.K-160 analytical balance (0.0001 g sensitivity), mixed for 10 minutes, and pressed in a 12 mm steel mold under 4 tons for 5 minutes, producing 3 mm-thick pellets.

Glass substrates were cleaned sequentially with acetone, ethanol, and deionized water for 15 minutes each, followed by drying at 60°C for 1 hour to remove contaminants and enhance film adhesion. Deposition was performed using a Nd:YAG pulsed laser ($\lambda = 1064$ nm, 10 ns pulse duration, 200 mJ, 6 Hz). The target–substrate distance was 2.5 cm, chamber pressure 2×10^{-3} Torr, and the laser beam was incident at 45° with 600 pulses per film. One pure CeO_2 film and three CNTs-doped films (0.1, 0.3, 0.5 wt.%) were deposited.

Deposited films were annealed at 350°C for 2 hours in a Renfert Magma 300 furnace (Germany), followed by a slow cool-down of 24 hours inside the furnace to enhance crystallinity and preserve CNTs structural integrity. The annealing conditions were selected based on CeO_2 crystallization and CNTs thermal stability.

The structural, morphological, and optical properties of thin films were analyzed using X-ray diffraction (XRD) for crystallinity and preferred orientation, Atomic force microscopy (AFM) for surface topography and grain size, scanning electron

microscopy (SEM) for morphology and grain distribution, and UV–Visible spectroscopy for optical absorption, from which the energy band gap was determined using Tauc's relation. The film thickness was also measured by an optical method and found to be approximately 200 nm.

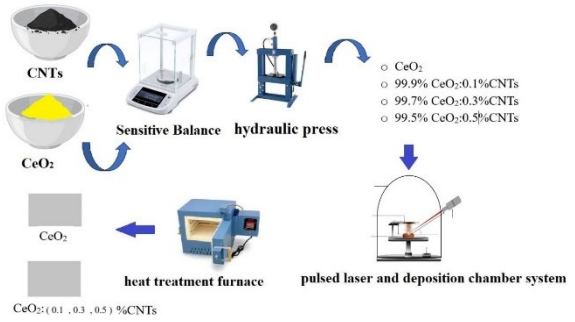

Fig. (1) A schematic illustrating the preparation method of cerium oxide films doped with CNTs

3. Results and discussion

Figure (2) shows the XRD patterns of pure and CNTs-doped CeO_2 thin films with doping ratios of 0.1, 0.3, and 0.5 wt.% CNTs. The pure CeO_2 film exhibits a polycrystalline cubic fluorite structure with diffraction peaks corresponding to the planes (111), (020), (022), (131), (222), (040), (133), (042), and (242), at 2θ diffraction angles of 28.41°, 32.83°, 47.54°, 56.95°, 58.94°, 69.91°, 76.98°, 79.87°, and 88.98°, respectively. The preferred orientation is along the (111) plane (2θ = 28.41°), consistent with standard JCPDS card no. 96-434-3151 [10].

Doping with CNTs did not alter the cubic fluorite structure, indicating that the CeO_2 phase remains stable. Slight shifts in the peak positions were observed, suggesting lattice strain induced by CNTs incorporation. Peaks corresponding to CNTs were not detected, likely due to their low concentration, amorphous nature, being below the XRD detection limit.

The crystallite size for the preferred plane in all prepared thin film was calculated using the Debye–Scherrer equation (1), and it was found that the crystallite size decreased with increasing doping ratio, as shown in table (1), where the crystallite size decreased significantly with CNTs doping, from 34.37 nm for the pure film to 11.74 nm for the 0.5 wt% CNTs-doped film. This is attributed to CNTs acting as nucleation centers, grain growth inhibitors, which may also pin grain boundaries, limiting crystal growth during annealing. This finding agrees with the results of researcher [11].

The lattice constant a, calculated for the (111) plane, showed slight variations: 5.425 Å for pure CeO_2, decreasing to 5.364 Å at 0.1% CNTs, then increasing to 5.493 Å at 0.3% and 5.463 Å at 0.5% CNTs. These variations indicate local strain or interfacial interactions between CNTs and CeO_2, with compressive strain at low doping and minor lattice expansion at higher doping levels, this agrees with [12]. Such interactions are consistent with the reduction in crystallite size and may influence the films' optical and electronic properties.

$$D = \frac{0.9\lambda}{\beta cos\theta} \quad (1)$$

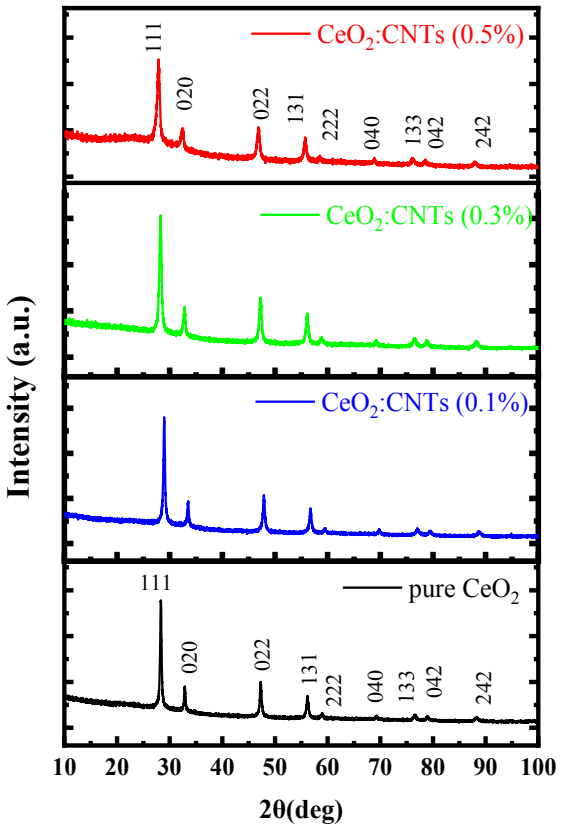

Fig. (2) XRD patterns of pure and CNTs-doped CeO_2 thin films

Studying the thin film surface is a crucial step in understanding how atoms are arranged and distributed on it. Figure (3) shows the atomic force microscopy (AFM) images of pure cerium oxide films and films doped with CNTs at different doping levels of (0.1, 0.3, and 0.5 wt.%). The images reveal the distribution of grains on the thin-film surface, where a noticeable decrease in the average grain size is observed with increasing CNTs content. The average grain size decreases from 250.35 nm for the pure film to 193.73 nm for the film doped with 0.5 wt.% CNTs, as listed in table (2).

In addition, the average surface roughness also decreases progressively with increasing CNTs doping, from 75.41 nm for the pure film to 32.524 nm for the film doped with 0.5 wt.% CNTs, as shown in table (2). This reduction in both grain size and roughness suggests that CNTs act as additional nucleation centers during film growth, leading to finer grains and a more compact surface morphology, which agrees with [13]. It is also observed that the grain size measured by AFM

is larger than the crystallite size obtained from XRD. This difference arises because AFM measures the size of surface grains, which may consist of several coherently scattering domains, whereas XRD measures the crystallite size inside the film.

Table (2) AFM analysis results showing surface roughness and grain size of pure and CNTs-doped CeO_2 thin films

Samples	Roughness Average (nm)	Grain Size Average (nm)
CeO_2 pure	75.413	250.35
CeO_2:0.1%CNTs	73.897	246.93
CeO_2:0.3%CNTs	58.897	216.05
CeO_2:0.5%CNTs	32.524	193.73

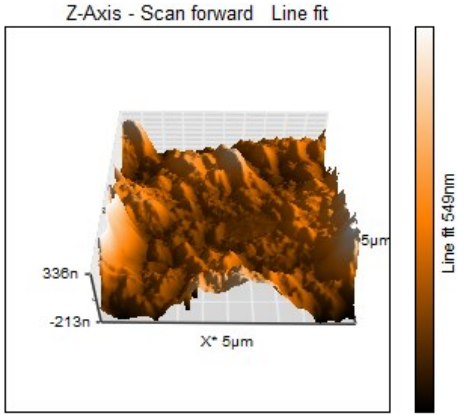

Pure CeO_2

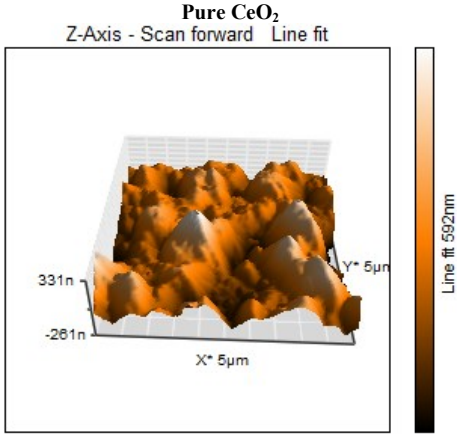

0.1% CNTs

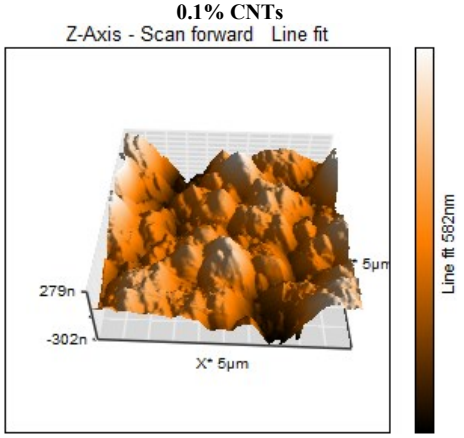

0.3% CNTs

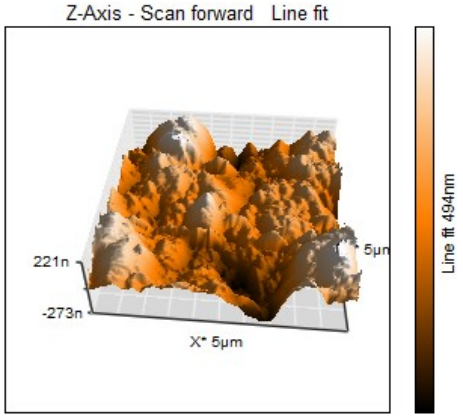

0.5% CNTs

Fig. (3) AFM images showing surface topography and grain size of pure and CNTs-doped CeO_2 thin films

Figure (4) shows SEM images of CeO_2 pure and CNTs-doped thin films. The images for pure indicate that the surface consists of interconnected, nearly spherical nanograins with relatively homogeneous grain distribution, although some regions exhibit grain agglomeration. This behavior suggests that the surface of the pure film is relatively rough. The grain diameters range between 32-72 nm. SEM images of CeO_2 films doped with 0.1 wt.% CNTs. The images demonstrate the effect of doping on the surface morphology, where the surface becomes less rough compared to the pure film. The grain distribution becomes slightly less homogeneous, with small grains appearing alongside larger ones. This behavior is attributed to the CNTs, which act as additional nucleation centers during grain growth. The grain size becomes relatively smaller than in the pure film, with grain diameters ranging between 44-60 nm. In SEM images of CeO_2 films doped with 0.3 wt.% CNTs. A noticeable increase in grain agglomeration is observed, with each cluster consisting of semi-spherical nanograins. The grain boundaries also become more distinct compared to previous films, indicating enhanced aggregation and less uniform grain growth. The average grain diameter further decreases, ranging between 31-53 nm. Where SEM images of CeO_2 films doped with 0.5 wt.% CNTs. The images indicate that CNTs doping leads to a surface consisting of closely packed nanograins with a more regular spatial distribution, although some localized agglomeration remains present. These agglomerates are most likely associated with CNTs-rich regions within the film. The average grain diameter ranges between 30-70 nm, which is consistent with the findings reported in [14].

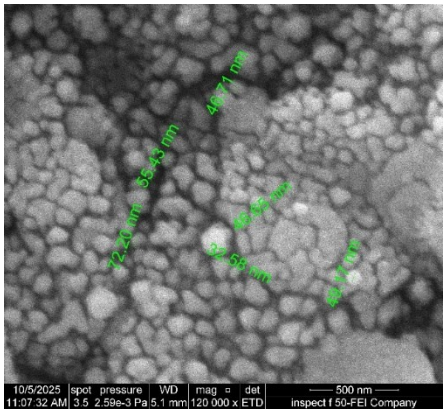

Pure CeO_2

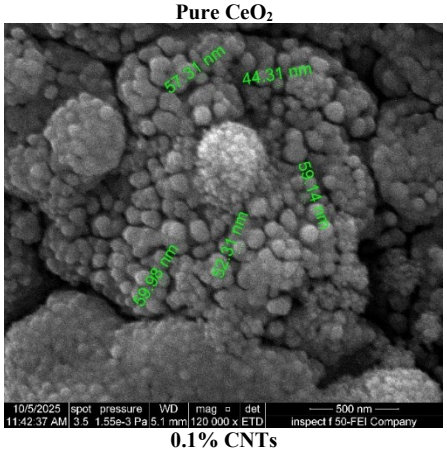

0.1% CNTs

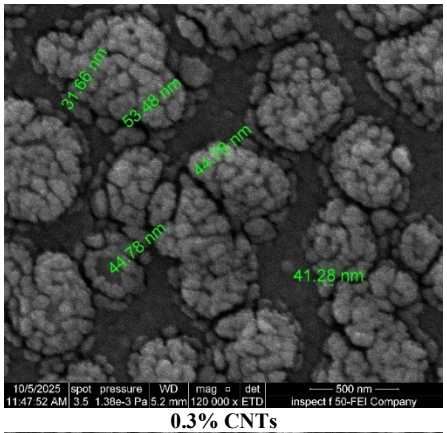

0.3% CNTs

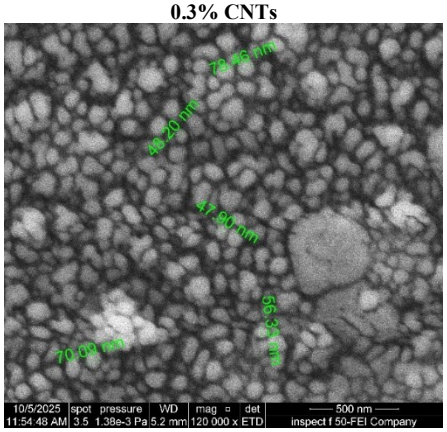

0.5% CNTs

Fig. (4) SEM images of pure and CNTs-doped CeO_2 thin films

Figure (5) shows the absorption spectrum as a function of wavelength for pure and CNTs-doped CeO_2 thin films with doping percentages of 0.1, 0.3, 0.5 wt.%, within the wavelength range of 300-1100 nm. The figure shows that absorbance is high in the ultraviolet region (300–400 nm) and gradually decreases with increasing wavelength. Furthermore, absorbance decreases with increasing doping percentage. This decrease in absorbance cannot be solely attributed to defect levels formed by CNTs, as such defect levels typically enhance absorption in the visible and near-IR regions by facilitating sub-band gap transitions. A more plausible explanation is the reduction in crystallite/grain size induced by CNTs doping, which increases grain boundary scattering and the surface-to-volume ratio, leading to higher reflection and consequently lower measured absorption. This explanation is consistent with the microstructural observations and agrees with [15].

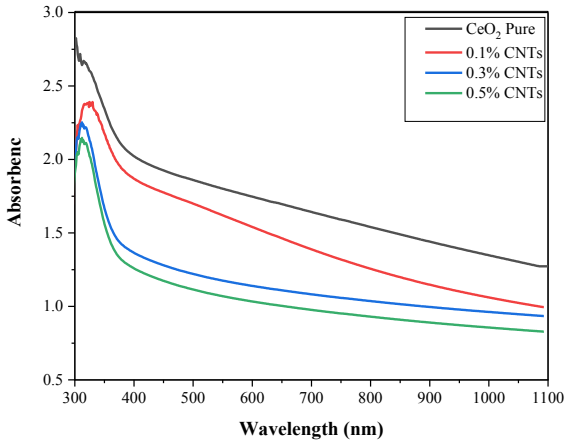

Fig. (5) Absorption spectra of pure and CNTs-doped CeO_2 thin films

Figure (6) shows the UV–Visible absorption coefficient of pure and CNTs-doped CeO_2 thin films with doping concentrations of 0.1, 0.3, and 0.5 wt.%. The absorption coefficient (α) is highest in the ultraviolet region (300–400 nm) for all samples and gradually decreases with increasing wavelength, indicating that the films strongly absorb UV light. Upon increasing the CNTs doping percentage, a clear reduction in absorption is observed across the entire measured range. This decrease can be attributed primarily to the reduction in crystallite and grain size caused by CNTs incorporation, which increases grain boundary scattering and enhances reflectance, thereby lowering the effective absorption. Additionally, while defect levels introduced by CNTs may facilitate sub-band gap transitions, their influence is outweighed by the quantum confinement effect arising from the reduced crystallite dimensions [16].

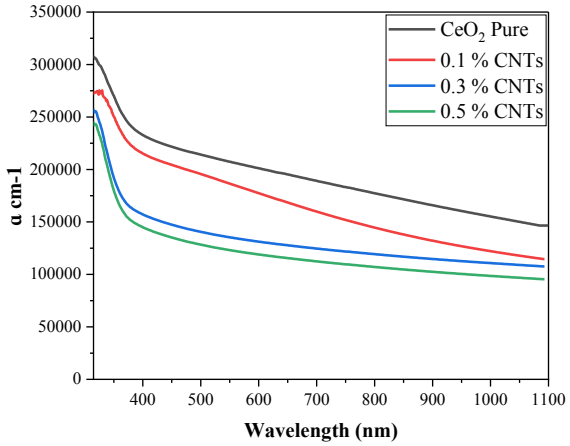

Fig. (6) The absorption coefficient of pure and CNTs-doped CeO_2 thin films

Figure (7) shows the graph of energy gap curves for pure and CNTs-doped CeO_2 thin films with doping percentages of 0.1, 0.3, 0.5 wt.%. It is noted from the figure that the energy gap increases with increasing doping percentages, rising from 2.71 eV for the pure thin film to 3.14 eV for the thin film doped with 0.5%, as shown in table (3).

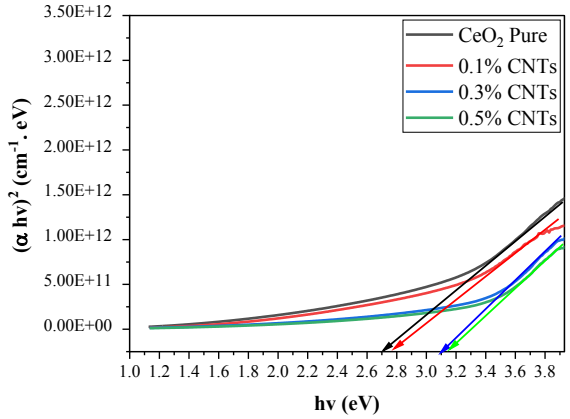

Fig. (7) Energy gap (E_g) curves of pure and CNTs-doped CeO_2 thin films

Table (3) Energy gap (E_g) values of pure and CNTs-doped CeO_2 thin films

Sample	Energy gap (eV)
CeO_2 pure	2.71
CeO_2:0.1%CNTs	2.78
CeO_2:0.3%CNTs	3.10
CeO_2:0.5%CNTs	3.14

The observed increase in the energy gap is primarily attributed to the quantum confinement effect (QCE), as the crystallite size decreases significantly with doping, confining electrons and holes in smaller spaces, increasing their energy and consequently widening the band gap. While the presence of CNTs may introduce secondary levels between the valence and conduction bands, which are generally expected to reduce energy bandgap, the dominant effect in this study appears to be QCE due to the size reduction into the quantum regime.

Several factors can influence the energy gap values, including the type of impurity material, membrane preparation method, doping process, deposition conditions, and the structural composition of the membranes, which agrees with [17,18].

4. Conclusions

Thin films of pure and carbon nanotubes (CNTs)-doped cerium oxide (CeO_2) were successfully prepared using the pulsed laser deposition technique. Doping with CNTs did not alter the crystal structure of the films; however, the crystallite size, calculated from the (111) plane at $2\theta = 28.41°$, decreased from 34.367 nm for the pure film to 11.740 nm for the film doped with 0.5% CNTs. This reduction in crystallite size was accompanied by a decrease in surface roughness, reaching 32.524 nm, while a corresponding decrease in grain diameter was confirmed. The optical properties of the films were also significantly affected by CNTs incorporation, as the energy gap increased to 3.14 eV primarily due to the quantum confinement effect. These results demonstrate that CNTs doping effectively modifies the structural, morphological, and optical properties of CeO_2 thin films. The findings suggest potential applications in UV-protective coatings, photocatalysis, and optoelectronic devices.

References

[1] I. Virt, "Recent advances in semiconducting thin films", *Coatings*, 13(1) (2023) 79.

[2] Z. Benzarti and A. Khalfallah, "Recent advances in the development of thin films", *Coatings*, 14(7) (2024) 878.

[3] R. Gaudiuso, "Pulsed laser deposition of carbon-based materials: a focused review of methods and results", *Processes*, 11(8) (2023) 2373.

[4] A. Alsaad et al., "Synthesized PANI/CeO_2 nanocomposite films for enhanced anti-corrosion performance", *Nanomater.*, 14(6) (2024) 526.

[5] R. Tan et al., "Breakthrough photothermal ammonia decomposition via low-barrier Ni-CeO_{2-x} interfaces on carbon nanotubes", *Nature Commun.*, 16 (2025) 11433.

[6] A. Hussain and Q. Abdullah, "Characterization of ZnO-SnO_2 nanostructures prepared by thermal evaporation technique as gas sensor", *Iraqi J. Appl. Phys.*, 19(4C) (2023) 243-250.

[7] K. Nguyen and M. Tran, "AFM analysis of ZnO thin films. Surf", *Interface Anal.*, 52(5) (2020) 234-240.

[8] P. Singh, "Band gap engineering in ZnO nanostructures", *Semicond. Sci. Technol.*, 35(4) (2020) 045001.

[9] S. Wang and V. Zhao, "Reflectance studies of CNTs ZnO films", *J. Appl. Phys.*, 127(12) (2020) 125301.

[10] Z. Bahtiar, T. Windarti and D. Hudiyanti, "The effect of calcination temperature on the characteristics of CeO_2 synthesized using the precipitation method", *Jurnal Kimia Sains dan Aplikasi.*, 27(5) (2024) 226-231.
[11] D. Channel et al., "Effect of iron doping on the structural and optical properties of CeO_2 films", *J. Sol-Gel Sci. Technol.*, 79(1) (2016) 126-133.
[12] K. Kumari et al., "Band gap engineering, electronic state and local atomic structure of Ni-doped CeO_2 nanoparticles", *J. Mater. Sci.: Mater. Electron.*, 30(7) (2019) 6370-6380.
[13] M. Michalska, K. Lemański and A. Sikora, "Spectroscopic and structural properties of CeO_2 nanocrystals doped with La^{3+}, Nd^{3+} and modified on their surface with Ag nanoparticles", *Heliyon*, 7(5) (2021) e06958.
[14] B. Zhao et al., "Yeast-template synthesized Fe-doped cerium oxide hollow microspheres for visible photodegradation of acid orange 7", *J. Colloid Interface Sci.*, 511 (2018) 39-47.
[15] D. Yang et al., "Investigation on the structural and photocatalytic performance of oxygen-vacancy-enriched SnO_2–CeO_2 heterostructures", *Int. J. Mol. Sci.*, 24(15) (2023) 15446.
[16] M. Ishaq and N. Qamhieh, "Study of optical energy gap and quantum confinement effects in Zinc Oxide nanoparticles and nanorods", *Digest J. Nanomater. Biostruct.*, 14(1) (2019) 119-125.
[17] C. Kumar, R. Pandeeswari and B. Jeyaprakash, "Structural, morphological and optical properties of spray-deposited Mn-doped CeO_2 thin films", *J. Alloys Compd.*, 602 (2014) 180-186.
[18] N. Ravindra, P. Ganapathy and J. Choi, "Energy gap–refractive index relations in semiconductors – An overview", *Infrared Phys. Technol.*, 50(1) (2007) 21-29.

Table (1) XRD results including crystallite size, lattice constant, d-spacing, and FWHM at the (111) plane for pure and CNT-doped CeO_2 thin films

Sample	2θ (deg)	FWHM (deg)	d-spacing (Å)	a (Å)	D (nm)	hkl	Height (cts)
CeO_2 pure	28.412	0.224	3.1323	5.425	34.367	111	1129.96
CeO_2:0.1%CNTs	28.530	0.335	3.0957	5.364	22.974	111	1617.13
CeO_2:0.3%CNTs	28.314	0.4772	3.1723	5.493	16.128	111	1493.46
CeO_2:0.5%CNTs	28.143	0.6552	3.1541	5.463	11.740	111	769.06

